On the Observed Relationships between Variability in Gulf Stream Sea Surface Temperatures and the Atmospheric Circulation over the North Atlantic

SAMANTHA M. WILLS AND DAVID W. J. THOMPSON

Department of Atmospheric Science, Colorado State University, Fort Collins, Colorado

LAURA M. CIASTO

Geophysical Institute, University of Bergen, and Bjerknes Centre for Climate Research, Bergen, Norway

(Manuscript received 17 November 2015, in final form 16 February 2016)

ABSTRACT

The advent of increasingly high-resolution satellite observations and numerical models has led to a series of advances in understanding the role of midlatitude sea surface temperature (SST) in climate variability, especially near western boundary currents (WBC). Observational analyses suggest that ocean dynamics play a central role in driving interannual SST variability over the Kuroshio–Oyashio and Gulf Stream extensions. Numerical experiments suggest that variations in the SST field within these WBC regions may have a much more pronounced influence on the atmospheric circulation than previously thought.

In this study, the authors examine the observational support for (or against) a robust atmospheric response to midlatitude SST variability in the Gulf Stream extension. To do so, they apply lead–lag analysis based on daily mean data to assess the evidence for two-way coupling between SST anomalies and the atmospheric circulation on transient time scales, building off of previous studies that have utilized weekly data. A novel decomposition approach is employed to demonstrate that atmospheric circulation anomalies over the Gulf Stream extension can be separated into two distinct patterns of midlatitude atmosphere–ocean interaction: 1) a pattern that peaks 2–3 weeks before the largest SST anomalies in the Gulf Stream extension, which can be viewed as the ''atmospheric forcing,'' and 2) a pattern that peaks several weeks after the largest SST anomalies, which the authors argue can be viewed as the ''atmospheric response.'' The latter pattern is linearly independent of the former and is interpreted as the potential response of the atmospheric circulation to SST variability in the Gulf Stream extension.

1. Introduction

The ocean is an integral part of the climate system, but its impact on the atmosphere varies greatly from one region of the globe to another. In the tropics, variations in sea surface temperatures (SST) are largely balanced by vertical motion (e.g., Hoskins and Karoly 1981). Hence, the linear atmospheric response to tropical SST anomalies can readily extend into the free-tropospheric circulation and have a notable impact on global climate (e.g., Horel and Wallace 1981). In contrast, variations in midlatitude SST anomalies are readily balanced by small changes in the horizontal wind field (e.g., Hoskins and Karoly 1981), and thus the linear atmospheric response to midlatitude SST anomalies may be relatively shallow and weak. Not surprisingly, the effects of midlatitude SST anomalies on the large-scale atmospheric circulation have proven difficult to isolate and quantify in both numerical experiments and observations, as summarized in the review by Kushnir et al. (2002).

Nevertheless, over the past decade, analyses of increasingly high-resolution satellite observations and numerical models have revealed a potentially more important role of the midlatitude ocean in extratropical climate than previously thought. The most robust effects of midlatitude SSTs on the large-scale atmospheric circulation have been found in the context of the *climatological-mean* circulation. Analyses of high-resolution SST and surface wind stress observations reveal that the climatological-mean near-surface wind field is strongly influenced by large horizontal gradients in the SST field, such as those associated with

Corresponding author address: Samantha M. Wills, Department of Atmospheric Science, Colorado State University, 3915 W. Laport Ave., Fort Collins, CO 80521.
E-mail: smwills@atmos.colostate.edu

DOI: 10.1175/JCLI-D-15-0820.1

the major western boundary currents (e.g., O'Neill et al. 2003; Nonaka and Xie 2003; Chelton et al. 2004; Chelton and Xie 2010). The associated patterns of convergence in the atmospheric boundary layer seemingly extend to vertical motion in the free troposphere and thus precipitation (e.g., Minobe et al. 2008, 2010). Results from numerical experiments run with and without sharp gradients in the SST field suggest that the climatological-mean ocean fronts play a key role in determining the location and amplitude of the extratropical storm tracks (e.g., Nakamura et al. 2008; Sampe et al. 2010; Small et al. 2014; Piazza et al. 2016).

To what extent *variability* in midlatitude SSTs influences the atmospheric circulation is less clear, but evidence is building that the influence may not be trivial. Observational analyses suggest that variations in SSTs in the vicinity of the Northern Hemisphere western boundary currents are linked to significant changes in the large-scale atmospheric circulation (e.g., Czaja and Frankignoul 2002; Ciasto and Thompson 2004; Frankignoul et al. 2011; Kwon and Joyce 2013). Numerical simulations imply that variations in midlatitude SST *gradients* are linked to changes in the amplitudes of the storm tracks (e.g., Brayshaw et al. 2008; Nakamura and Yamane 2009; Hand et al. 2014; O'Reilly and Czaja 2015). Importantly, a very recent numerical experiment suggests that the atmospheric response to midlatitude SST anomalies may vary dramatically depending on the spatial resolution of the atmospheric model (e.g., Smirnov et al. 2015): in a low-resolution version of the Community Atmosphere Model, version 5 (CAM5) atmospheric general circulation model, the atmospheric response to midlatitude SST anomalies is dominated by horizontal temperature advection in the lowermost troposphere, but in a high-resolution version, it includes substantial changes in vertical motion and thus potentially the hemispheric-scale circulation. The link between variations in midlatitude SSTs and vertical motion is also found in numerical experiments of the extratropical storm response to SST anomalies (e.g., Czaja and Blunt 2011; Sheldon and Czaja 2013).

The goal of this contribution is to reexamine the observational evidence for midlatitude ocean–atmosphere interaction, with a focus on variations in SSTs over the Gulf Stream extension. We exploit daily mean data to examine the lead–lag relationships between variability in the atmospheric circulation and SST variability in the Gulf Stream extension on subseasonal time scales. The key novel result is that SST anomalies in the Gulf Stream extension are associated with two distinct and independent patterns of atmospheric variability: 1) a pattern that leads the SST field and is interpreted as the atmospheric forcing of the SST anomalies and 2) a pattern that lags the SST field and is interpreted as the atmospheric response. The former pattern is expected and is consistent with previous results. As far as we know, the latter pattern has not been documented in association with atmosphere–ocean interaction over the North Atlantic. Section 2 describes the data. Section 3 explores the patterns of atmospheric variability associated with variations in SSTs over the Gulf Stream extension. Section 4 provides a physical interpretation of the results. Conclusions are provided in section 5.

2. Data

All results are based on daily mean output from the 1.5°-resolution ERA-Interim (e.g., Dee et al. 2011; http://apps.ecmwf.int/datasets/data/interim-full-daily/levtype=sfc/) dataset over the 35-yr period 1979–2013. Anomalies of SST, potential temperature (θ), wind ($\mathbf{v}$), and geopotential height (Z) were formed by removing the long-term mean seasonal cycle from the data. The data are detrended to remove the influence of trends on the results (in practice, the results are roughly the same whether the data are detrended or not). Throughout the study, SLP is expressed as geopotential height at 1000 hPa (Z_{1000}), as depicted in the figures. Note that sea surface temperature is a prescribed boundary condition in ERA-Interim and is a collection of several different observational data products (e.g., Dee et al. 2011, cf. their Table 1). As noted in the text, key results are reproduced using SST data from the NOAA optimum interpolated dataset (e.g., Reynolds et al. 2002). Apart from the removal of the seasonal cycle and the detrending, the data are not filtered in any way in the analyses.

3. Observed lead–lag relationships between the atmospheric circulation and SSTs in the Gulf Stream extension

Figure 1 reviews key aspects of the climatological-mean circulation and SST field over the North Atlantic during the NH winter months of December–February (DJF). Figure 1a shows the DJF-mean SST and 850-hPa wind fields; Fig. 1b shows the standard deviation of daily mean SST anomalies during DJF. As noted extensively in previous studies (e.g., Nakamura et al. 1997; Nonaka and Xie 2003; Ciasto and Thompson 2004; Deser et al. 2010; Smirnov et al. 2014, etc.), the standard deviation of midlatitude SSTs peaks in the region of largest horizontal temperature gradients. Variations in SSTs in the Gulf Stream region and its extension can arise from forcing by the atmospheric flow, particularly in association with temperature advection from the cold continental regions to the west (e.g., Frankignoul 1985; Haney 1985; Kushnir et al. 2002). They can also arise from forcing by the ocean circulation itself, especially near western boundary currents (e.g., Frankignoul and Reynolds 1983; Smirnov et al. 2014). The focus of this paper is on the two-way

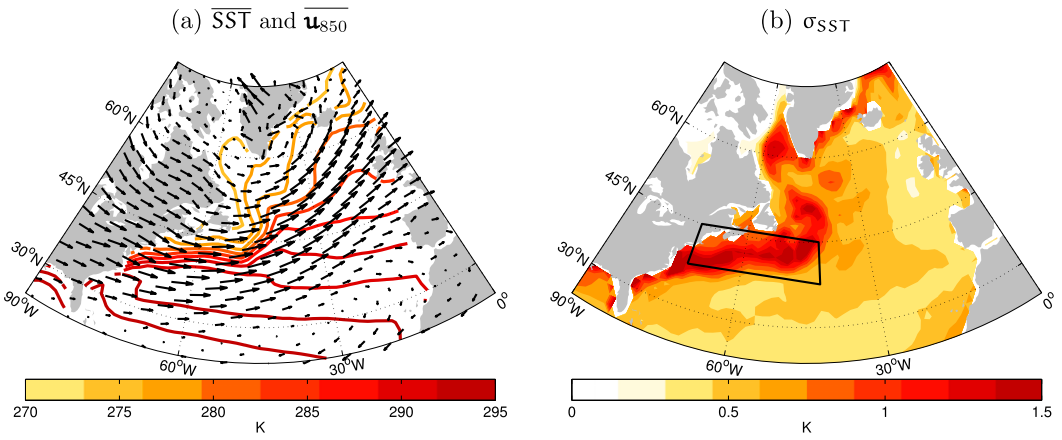

FIG. 1. North Atlantic wintertime (DJF) (a) climatological-mean SST (contours) and $\mathbf{u}_{850}$ (vectors) and (b) standard deviation of SST (σ_{SST}). The boxed region spans 37.5°–45°N, 72°–42°W and indicates the region used to calculate the G_{SST} index. Units for SST and σ_{SST} are in K. Units for $\mathbf{u}$ are in m s^{-1}.

interactions between the large-scale atmospheric circulation and SST anomalies over the region of large SST variance in the Gulf Stream extension (Fig. 1b).

To investigate the linkages between the atmospheric circulation and SSTs in the Gulf Stream extension, we first generate a time series of daily mean SST anomalies averaged over the region 37.5°–45°N, 72°–42°W (indicated by the box in Fig. 1b). The index (hereafter G_{SST}) is standardized so that it has a mean of zero and standard deviation of one. By construction, positive values of the index correspond to warmer-than-normal SSTs in the Gulf Stream extension, and vice versa. We then compute lag relationships between various fields and the G_{SST} index using daily mean data. Note that the results are not sensitive to the specific domain used to define the Gulf Stream extension.

The left column in Fig. 2 shows daily mean SST (shading) and SLP (contours) anomalies regressed onto the G_{SST} index time series as a function of lag. Negative lags indicate results where the SLP and SST fields precede peak amplitude in the G_{SST} index, and vice versa for positive lags. The G_{SST} index is always centered on the 90-day period from 1 December to 28 February, whereas the fields being regressed shift from 11 November–8 February (for the lag −20 regressions) to 21 December–20 March (for the lag +20 regressions). The statistical significance of the SLP anomalies at negative and positive lags is indicated in Fig. 3.

The SST regression coefficients shown in the left column of Fig. 2 indicate the evolution of the SST field. By construction, the SST anomalies peak at lag 0 and in the vicinity of the Gulf Stream extension. The amplitudes of the SST anomalies are comparable to the standard deviations in Fig. 1b (also by construction since the G_{SST} index is standardized). They decay slowly with increasing lag, consistent with the relatively large thermal inertia of the ocean mixed layer.

The SLP regression coefficients indicate the attendant evolution of the atmospheric circulation. The most pronounced circulation anomalies are found at negative lags (i.e., the atmosphere leading variations in G_{SST}), when positive SLP anomalies span much of the North Atlantic basin. As indicated in previous analyses based on pentad and weekly mean SST data (e.g., Deser and Timlin 1997; Ciasto and Thompson 2004), the SLP anomalies at negative lags are consistent with forcing of the SST field by anomalies in the atmospheric circulation. In regions of large SST gradients (Fig. 1a), periods of anomalously warm SSTs over the Gulf Stream extension are consistent with anomalously southerly flow (Fig. 2, top panels in left column), and vice versa.

While the large SLP anomalies that lead variations in G_{SST} are entirely expected, the SLP anomalies that lag variations in G_{SST} are more intriguing. The regressions suggest that the several week period following anomalously warm conditions in the Gulf Stream extension is marked by anomalously low SLP over the Gulf Stream region and anomalously high SLP centered to the south of Iceland. The pattern of SLP anomalies at positive lags is statistically significant at the 95% confidence level (Fig. 3) and reproducible in other datasets (i.e., the NOAA optimum interpolated dataset, not shown). Importantly, the anomalous circulations leading and lagging variations in G_{SST} have distinct spatial structures, as quantified below.

The differences between the patterns of SLP anomalies that precede and follow variations in G_{SST} are quantified using a linear decomposition method as follows. First, we define the pattern of SLP anomalies at lag −20 as the "atmospheric forcing" pattern (hereafter denoted SLP_{-20}).

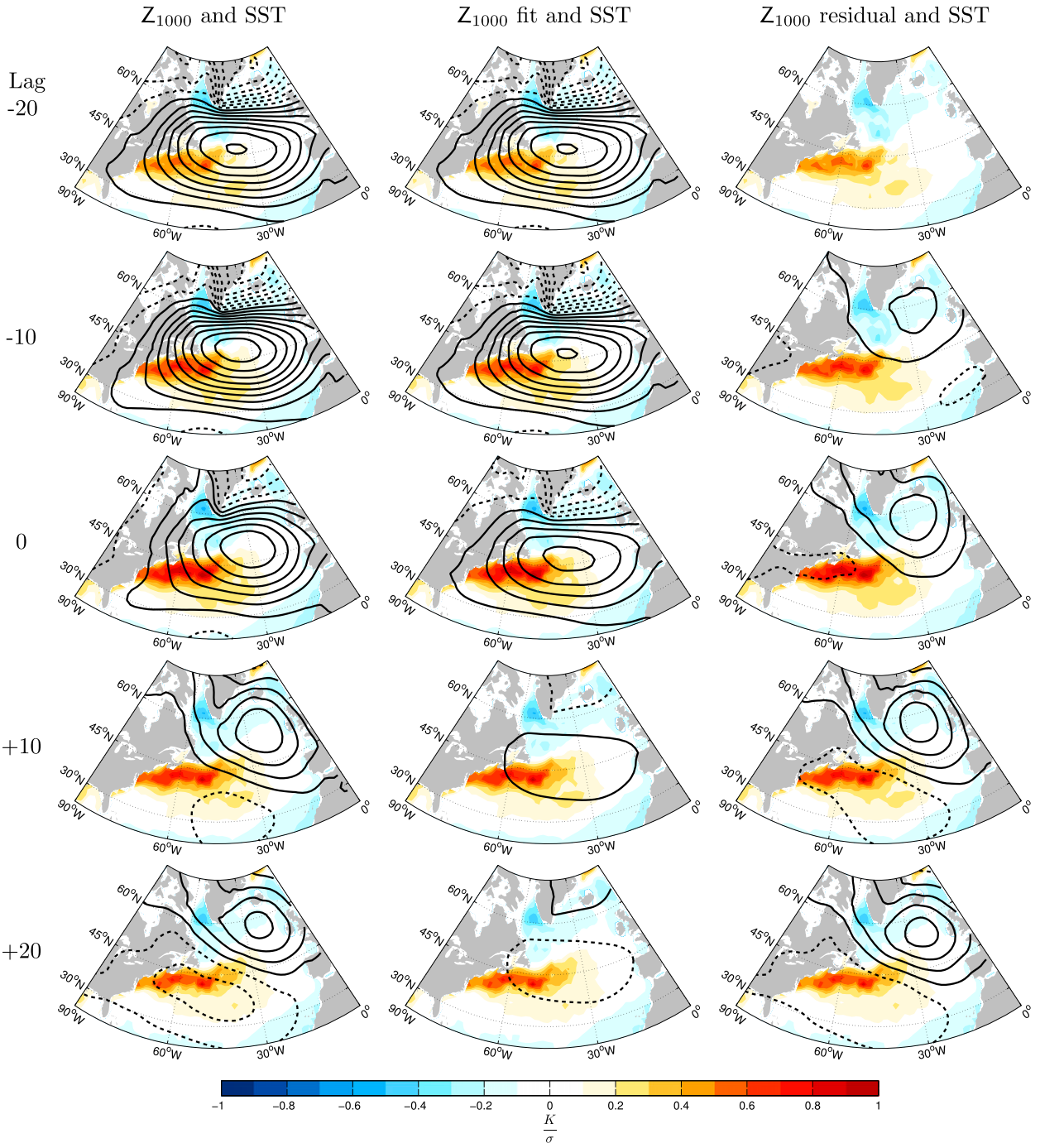

FIG. 2. (left) Wintertime lag regressions of Z_{1000} (contours) and SST (shading) onto the standardized G_{SST} index, with negative (positive) lags denoting Z_{1000}/SST anomalies leading (lagging) G_{SST}. (middle and right) Linear decomposition of Z_{1000} where the anomalous field is decomposed into two parts: (middle) the linear fit of Z_{1000} to the total −20-day lag regression map and (right) the residual Z_{1000}. The total SST regression at each lag is shown in all three columns. Z_{1000} contours are spaced at 4 m (−6, −2, 2, 6, ... m), where solid (dashed) lines indicate positive (negative) anomalies. Note that for Z_{1000} at each lag, $\text{map}_{\text{left}} = \text{map}_{\text{middle}} + \text{map}_{\text{right}}$.

We then decompose the SLP regression maps at all lags into two components: 1) a pattern that is linearly congruent with the atmospheric forcing pattern (i.e., the "fit" to SLP_{-20}) and 2) a "residual" pattern that is linearly independent of the SLP_{-20} regression map. That is, the SLP regression map at lag t is given as

$$\text{SLP}_t = \alpha_t \text{SLP}_{-20} + \text{SLP}_t^*, \quad (1)$$

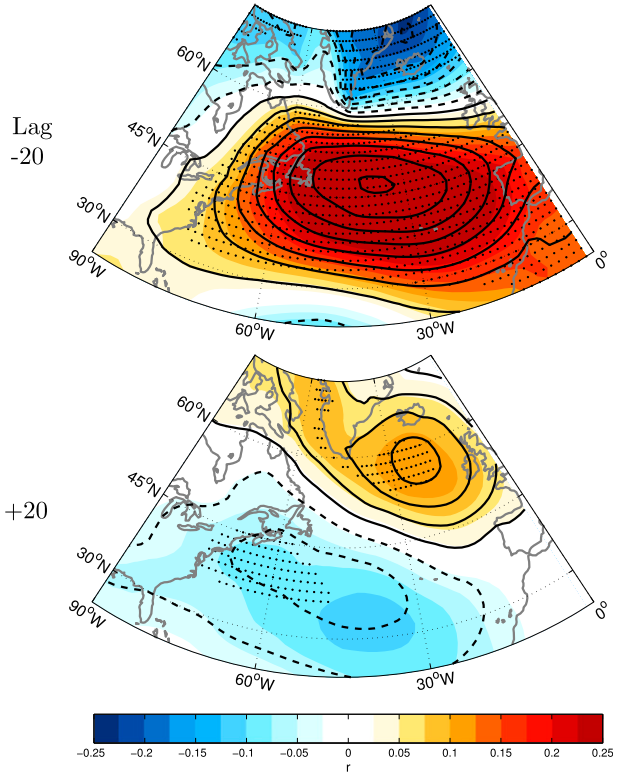

FIG. 3. Regressions (contours) and correlations (shading) of Z_{1000} against the standardized G_{SST} index at a lag of (top) −20 days and (bottom) +20 days. Stippling indicates significance at the 95% confidence level using the two-tailed Student's t test. Degrees of freedom are calculated per Eq. (31) from Bretherton et al. (1999), using the observed autocorrelations of the G_{SST} index (~60 days) and Z_{1000} (~10 days).

where SLP_t is the total SLP regression map at lag t, α_t is the spatial regression coefficient found by projecting SLP_t onto SLP_{-20} (α varies as a function of lag), and SLP_t^* is the residual SLP pattern at lag t.

The middle column of Fig. 2 shows the components of the SLP regressions that are linearly congruent with (or "fitted" to) SLP_{-20} (i.e., the middle column shows the evolution of the atmospheric forcing pattern as given by $\alpha_t SLP_{-20}$). The SST anomalies are reproduced from the left column. By construction, at all lags the patterns in the middle column are identical to the total regression at lag −20 and vary only in amplitude. The amplitude of the atmospheric forcing pattern decays on a time scale of several weeks, and has only weak amplitude at positive lags.

The right column in Fig. 2 shows the components of the SLP regressions that are linearly independent of SLP_{-20} (i.e., the column shows the residual SLP patterns given by SLP_t^*). Note that the spatial correlation coefficient between SLP_t^* and SLP_{-20} is zero at all lags; hence, the SLP_t^* maps reflect the components of the regressions that are linearly independent of the atmospheric forcing pattern.

The residual SLP patterns in the right column are not constrained to have similar spatial structure at all lags, *but they do*. This is important since it suggests that the space/time evolution of SLP anomalies associated with variations in SSTs in the Gulf Stream extension region can be viewed as the superposition of two structures: 1) a pattern that peaks in amplitude during the 10–20-day period before peak amplitude in the G_{SST} index and is consistent with forcing of the SST field by the atmospheric circulation (middle column of Fig. 2), and 2) a linearly independent pattern of SLP variability that grows in amplitude from ~lag 0 through the several week period after peak amplitude in the G_{SST} index (right column of Fig. 2; the anomalies peak in amplitude near lag +15 days, not shown). Both patterns are statistically significant, as shown in Fig. 3 (details of the significance tests are provided in the caption). As noted above and explored in section 4, the former pattern is consistent with atmospheric forcing of the SST field via anomalous temperature advection by the anomalous horizontal flow. In the next section, we will argue that the latter pattern may be interpreted as the "atmospheric response" to the underlying SST anomalies.

Figure 4 explores the associated time-varying structures in the 500-hPa geopotential height (Z_{500}) and 850-hPa potential temperature (θ_{850}) fields. The figure is constructed in an identical manner to Fig. 2, but in this case the analyses and decomposition procedure are based on lag regressions between Z_{500} anomalies and the G_{SST} index (contours) and between θ_{850} anomalies and the G_{SST} index (shading). The results in Fig. 4 indicate that the patterns of atmospheric variability that lead and lag G_{SST} both include a barotropic component. That is, the circulation anomalies are vertically stacked and increase in strength with height. The results in Fig. 4 also indicate that the temperature changes in the lower troposphere lie directly over the SST anomalies when the atmosphere leads G_{SST}, but are shifted to the northeast of the SST anomalies when the atmosphere lags G_{SST}. As noted in the following section, the structure of the lower-tropospheric temperature anomalies may provide an important clue regarding the development of the circulation anomalies that follow variations in G_{SST}.

4. Discussion

The results in Figs. 2–4 suggest that wintertime SST variability in the Gulf Stream extension is associated with two, linearly independent patterns of atmospheric variability: 1) a pattern of circulation anomalies that

peaks prior to largest amplitude in the SST field and 2) a very different pattern of circulation anomalies that peaks after largest amplitude in the SST field. The linear independence of the two patterns is highlighted by the decomposition applied in the middle and right columns of Figs. 2 and 4. But in practice, the linear decomposition is not required to identify the pattern of circulation anomalies that lags G_{SST} (i.e., the lower-left and lower-right panels in Figs. 2 and 4 are nearly identical). In this section, we explore key aspects of the pattern of circulation anomalies that forms during the period of several weeks after largest amplitude in the G_{SST} time series.

a. Comparison with results based on an atmospheric index

There are at least two possible physical explanations for the pattern of atmospheric circulation anomalies that lags G_{SST}: 1) the pattern may simply reflect the evolution of the atmospheric circulation that would occur even in the absence of the underlying SST anomalies; or 2) the pattern may reflect the response of the atmospheric circulation to SST anomalies in the Gulf Stream extension. To test against the former possibility, we repeated the analyses in Fig. 2, but for regressions based on the expansion coefficient time series of the SLP_{-20} regression map. The expansion coefficient time series was formed by projecting daily mean SLP anomalies onto the SLP_{-20} map on all days of the analysis and then standardizing the resulting index. By construction, the time series (hereafter G_{atmos}) indicates the temporal evolution of the SLP pattern shown in the top-left panel of Fig. 2. Lag regressions of SST and SLP onto the G_{atmos} time series were then calculated for lags spanning 0 to +40 days. The SLP regressions hence indicate the time evolution of the SLP_{-20} pattern with no (direct) information from the SST field. The lags range from 0 to 40 days so that the results can be compared directly with those based on the G_{SST} time series (i.e., lag 0 in the G_{atmos} time series corresponds to lag −20 in the G_{SST} time series).

Figure 5 shows the results of the regression analysis. The SLP anomalies associated with G_{atmos} decay over roughly 1–2 weeks, consistent with the *e*-folding time scale of G_{atmos} (~10 days) and the results in the middle column of Fig. 2. However, results based on the G_{atmos} time series differ from those based on the G_{SST} time series in two important ways: 1) the SST anomalies derived from regressions onto G_{atmos} are relatively weak, which suggests a substantial fraction of the variance in the SST field is unrelated to this particular pattern of SLP forcing; and 2) the SLP anomalies associated with the G_{atmos} time series do not evolve into a pattern of circulation anomalies reminiscent of the structure that lags peak amplitude in G_{SST}. Hence, the pattern of residual SLP anomalies observed at positive lags in Fig. 2 does not appear to simply reflect the evolution of the atmospheric circulation. Rather, it is seemingly dependent on the inclusion of information from the SST field itself.

b. Signature in temperature advection

What physical processes might give rise to the pattern of SLP anomalies at positive lag? Here we argue that they may reflect the circulation response to the poleward and upward advection of anomalously warm air from the Gulf Stream extension.

As shown in Fig. 4, the circulation anomalies associated with G_{SST} are accompanied by two distinct patterns of lower-tropospheric temperature anomalies: 1) positive temperature anomalies that overlie the Gulf Stream extension during the weeks preceding variations in G_{SST}; and 2) positive temperature anomalies to the northeast of the Gulf Stream extension during the weeks following variations in G_{SST}. As shown below, the former temperature anomalies are consistent with temperature advection by the *anomalous* circulation across the *climatological-mean* gradients in lower-tropospheric temperature, whereas the latter are in part dependent on temperature advection by the *climatological-mean* circulation across the *anomalous* gradients in temperature. As such, the former are not dependent on the existence of anomalies in the SST field, but the latter are dependent.

The relative roles of temperature advection by the anomalous and climatological-mean atmospheric circulations can be quantified by decomposing the total anomalous horizontal temperature advection at 850 hPa as follows:

$$(\mathbf{u}\cdot\nabla\theta)_{TOT} = \underset{\text{(I)}}{\mathbf{u}_A\nabla\theta_C} + \underset{\text{(II)}}{\mathbf{u}_C\nabla\theta_A} + \underset{\text{(III)}}{\mathbf{u}_A\nabla\theta_A}, \qquad (2)$$

where $\mathbf{u}$ and θ represent the horizontal components of the wind and potential temperature at 850 hPa, respectively; C denotes the climatological mean; and A denotes the anomalies. The total anomalous temperature advection is given by the left-hand side (lhs) and the terms on the right-hand side (rhs) denote (I) advection by the anomalous flow across the climatological-mean temperature gradients, (II) advection by the climatological-mean flow across the anomalous temperature gradients, and (III) advection by the anomalous flow across the anomalous temperature gradients.

Figure 6 shows the patterns of temperature advection associated with all three terms at lag 0. The top panel

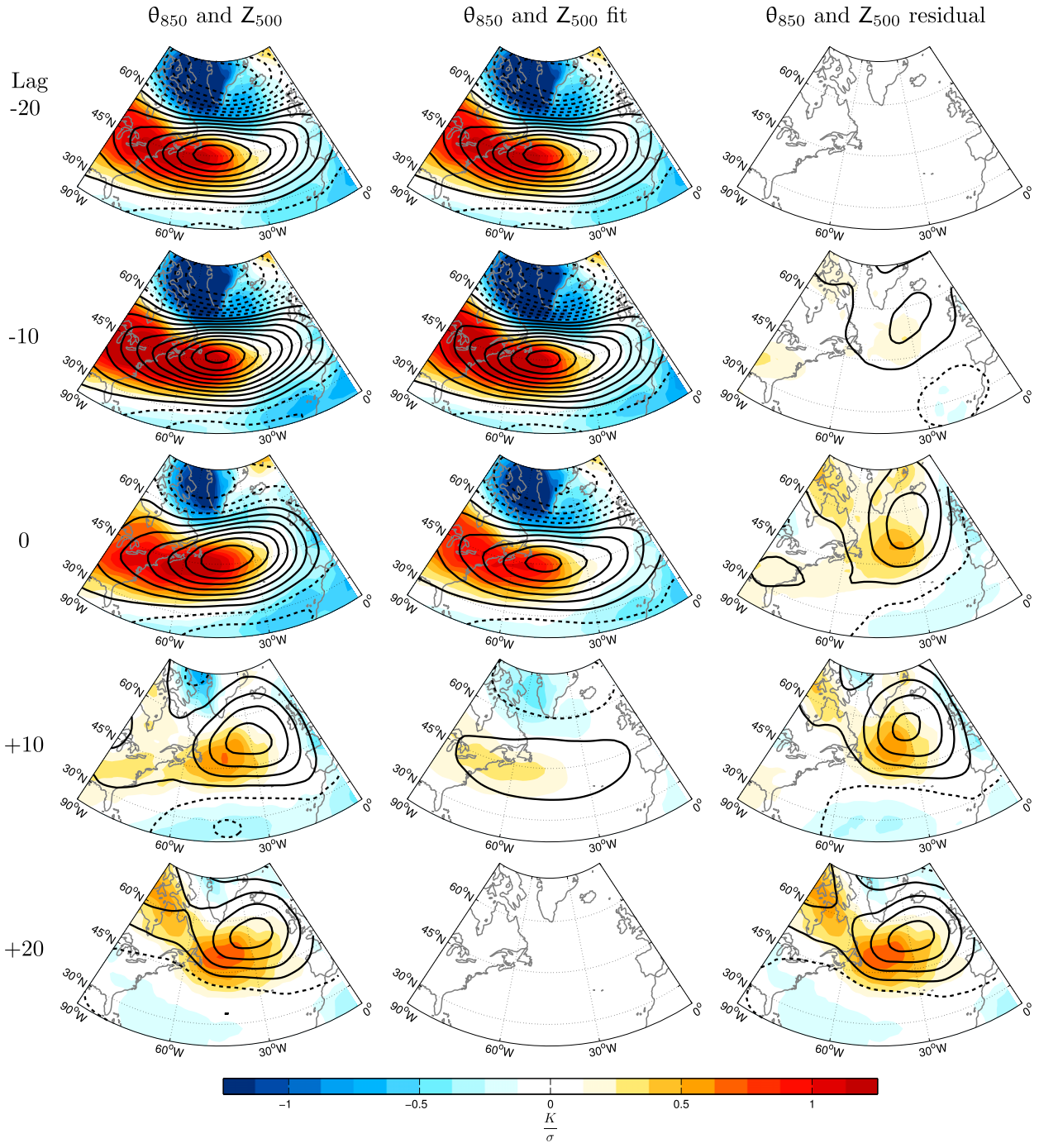

FIG. 4. As in Fig. 2, but for the linear decomposition of both θ_{850} (shading) and Z_{500} (contours). The Z_{500} contours are spaced at 6 m (−9, −3, 3, 9, . . . m).

shows results for the first term on the rhs of Eq. (2). Contours indicate the climatological-mean isotherms at 850 hPa, vectors indicate the anomalous flow at 850 hPa, and shading indicates the associated anomalous temperature advection. As inferred in section 3, advection by the anomalous flow across the climatological-mean temperature gradients gives rise to a pattern of temperature tendencies at 850 hPa that peaks over the region of largest SST anomalies, consistent with forcing of the SST field by the anomalous atmospheric circulation.

The middle panel of Fig. 6 shows results for the second term on the rhs of Eq. (2). Here, contours

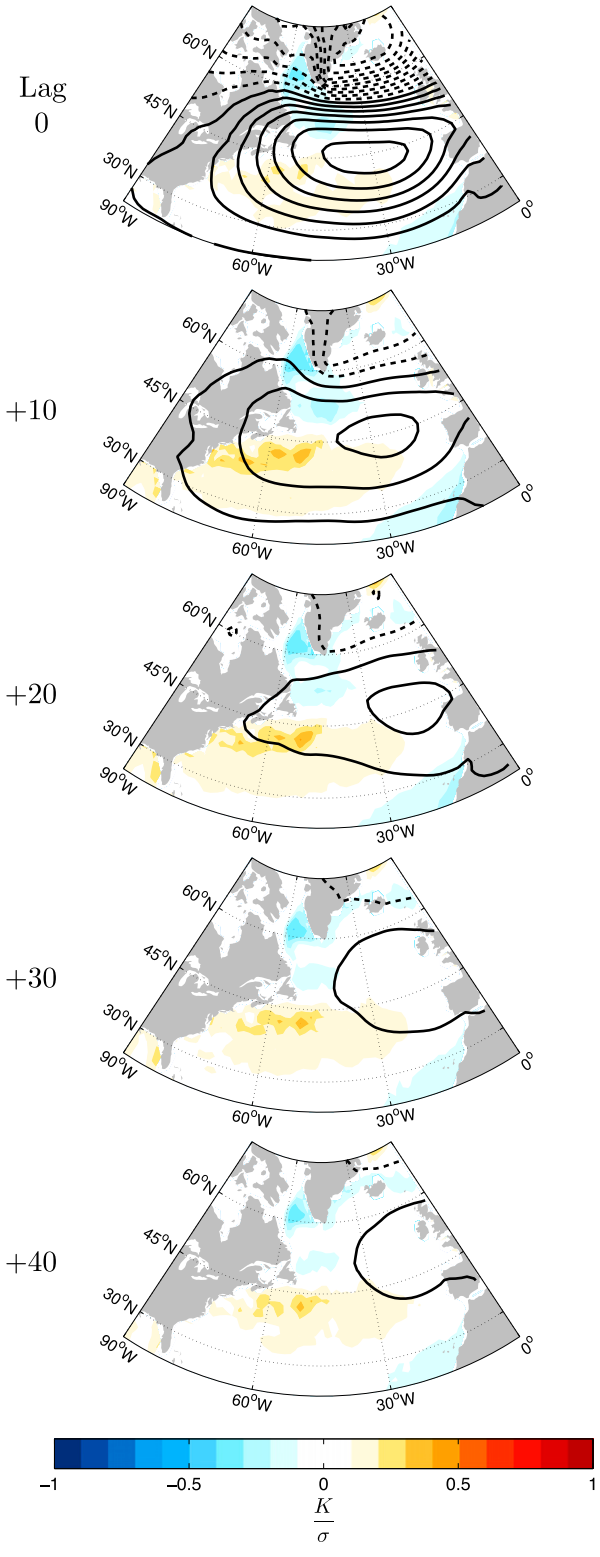

FIG. 5. Daily lag regressions of SST (shading) and Z_{1000} (contours) onto the standardized G_{atmos} index. The Z_{1000} contours with solid (dashed) lines represent positive (negative) values at an interval spacing of 10 m (−15, −5, 5, 15, ... m). Positive lags indicate the Z_{1000}/SST anomalies lagging the G_{atmos} index.

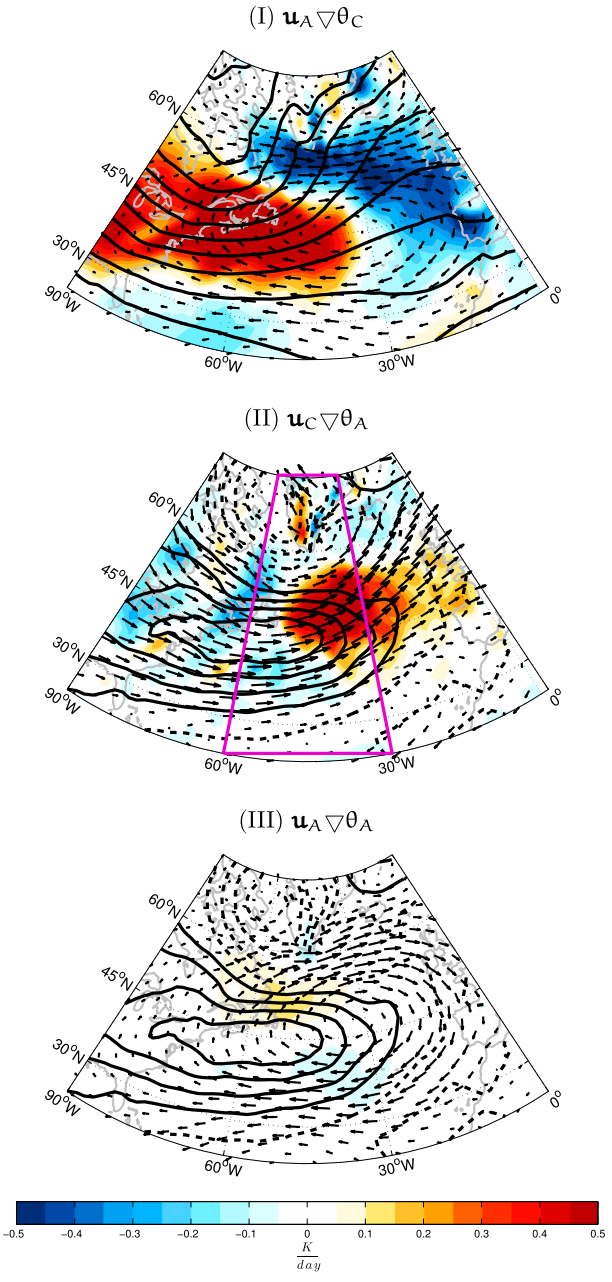

FIG. 6. The 850-hPa wintertime patterns of anomalous horizontal temperature advection associated with all three terms on the rhs of Eq. (2) at lag 0: (I) advection of the climatological-mean temperature gradient by the anomalous flow, (II) advection of the anomalous temperature gradient by the climatological-mean flow, and (III) advection of the anomalous temperature gradient by the anomalous flow. Contours represent the spatial temperature distribution, vectors represent the wind, and shading represents temperature advection. Units for SST, **u**, and temperature advection are in K, m s^{-1}, and K day^{-1}, respectively. The purple box in (II) indicates the region averaged for the cross section in Fig. 7.

indicate the 850-hPa temperature anomalies, vectors indicate the climatological-mean flow at 850 hPa, and shading indicates the associated temperature advection. Advection by the climatological-mean flow across the anomalous temperature gradients gives rise to a very different pattern of temperature tendencies than that shown in the upper panel. The anomalous temperature advection in the middle panel has comparable amplitude to that in the top panel, but projects onto the atmospheric temperature and circulation anomalies over the central North Atlantic rather than the Gulf Stream extension. Since it is dependent on the *anomalies* in lower-tropospheric temperature, the pattern of temperature tendencies in the middle panel of Fig. 6 (and thus the lower-tropospheric temperature anomalies over the North Atlantic following G_{SST}) derive from the warming of the lower troposphere over the Gulf Stream region.

The bottom panel of Fig. 6 shows the corresponding results for the third term on the rhs of Eq. (2). Advection by the anomalous flow across the anomalous temperature gradients has a relatively small contribution to temperature advection in the lower troposphere.

c. *Signature in vertical motion and the hemispheric-scale circulation*

To the extent that the underlying SST field influences variations in lower-tropospheric temperatures over the Gulf Stream extension, it follows that the pattern of temperature advection in the middle panel of Fig. 6 may be at least partially attributed to the underlying temperature anomalies in the SST field. Figure 7 reveals that the resulting positive temperature anomalies over the central North Atlantic during the period following peak amplitude in G_{SST} are also associated with anomalous rising motion.

Figure 7 shows meridional and vertical circulation anomalies regressed on G_{SST} at lag +20 (i.e., when the atmosphere lags the ocean) over the boxed region indicated in the second panel of Fig. 6. The warming to the northeast of the Gulf Stream extension is marked by positive temperature anomalies that extend throughout the atmospheric column at positive lag. Notably, the positive temperature anomalies also coincide with anomalous upward motion between ~45° and 60° latitude. The anomalous rising motion is consistent with results by Smirnov et al. (2015), who noted that SST anomalies over the Kuroshio–Oyashio Extension are associated with warm, rising air when the atmosphere lags the SST field by several weeks. Similar results were also noted by Czaja and Blunt (2011) and Sheldon and Czaja (2013), who argued that SST-induced heating in the Gulf Stream region can be

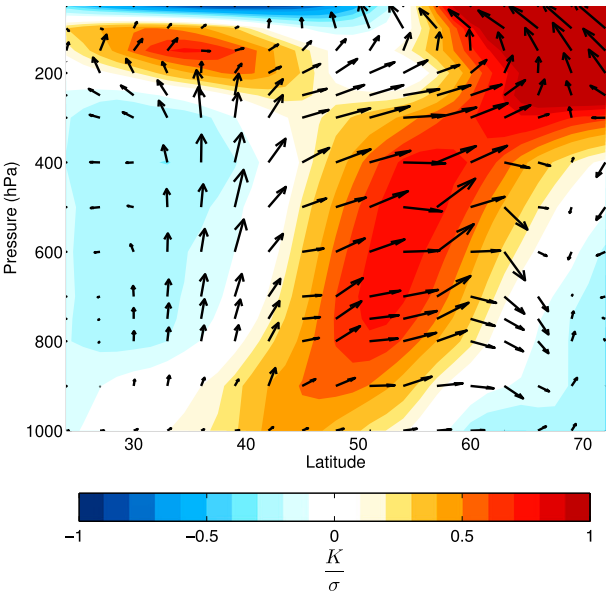

FIG. 7. The 60°–30°W averaged vertical cross section of θ (shading) and **v**, **w** (vectors) regressed onto the standardized G_{SST} index at a lag of +20 days. The **v**, **w** vectors are in units of m s^{-1}, with w scaled by a factor of 2×10^3 for qualitative comparison.

advected upward and poleward in the warm sector of extratropical storms.

The anomalous rising motion indicated in Fig. 7 is important for three reasons. One, the coexistence of heating and rising motion indicates that anomalous heating may be viewed as forcing, rather than responding, to the changes in vertical motion (if the anomalous motion was downward, then the positive temperature anomalies in the free troposphere would be consistent with adiabatic compression). Two, it suggests that the heating due to extratropical SST anomalies is being balanced, at least in part, by anomalous vertical motion. A similar conclusion was reached by Smirnov et al. (2015) in their simulations of the atmospheric response to Kuroshio–Oyashio Extension SST anomalies. Third, the changes in vertical motion suggest that the anomalous heating of the lower troposphere in regions to the northeast of the Gulf Stream extension extends to the upper-tropospheric circulation.

If the heating of the lower troposphere by the SST field is balanced by vertical motion, it follows that it will lead to the generation of circulation anomalies at upper-tropospheric levels. As demonstrated in Fig. 4, the lower-tropospheric heating anomalies to the northeast of the Gulf Stream extension are, in fact, associated with higher-than-normal geopotential heights at 500 hPa, consistent with hydrostatic balance of the column of air. As shown in Fig. 8, the free-tropospheric geopotential height anomalies associated with G_{SST} also appear to extend downstream beyond the Gulf Stream extension.

Figure 8 shows the regressions of the Z_{500} and SST (top) and SLP and SST (bottom) fields onto the G_{SST} index at lag +20 for the entire hemisphere. The results are identical to the SLP and Z_{500} results shown in Figs. 2 and 4, but include regression coefficients beyond the North Atlantic sector. The pattern of circulation anomalies associated with G_{SST} is consistent with a wave train extending across much of Europe and western Russia. A very similar pattern of geopotential height anomalies was recently found in Cui et al. (2015) in their analysis of covariability between climate variability over central Asia and the North Atlantic sector.

5. Conclusions

The results in this study suggest that SST variability in the Gulf Stream extension is associated with two distinct patterns of tropospheric circulation anomalies: 1) a pattern that peaks in amplitude several weeks before the largest anomalies in Gulf Stream extension SSTs, and is consistent with forcing of the SST field by the anomalous atmospheric circulation; and 2) a very different pattern that peaks in amplitude several weeks after the largest anomalies in Gulf Stream extension SSTs. As far as we know, the latter pattern has not been identified in previous observational analyses of atmosphere–ocean interaction of the North Atlantic sector. Lead–lag regressions do not prove causality, but several observations suggest that the pattern of circulation anomalies that lag the SST field may reflect the atmospheric response to SST anomalies in the Gulf Stream region: the pattern of circulation anomalies at positive lags has a very different spatial structure than the pattern at negative lags (Fig. 2), it is statistically significant (Fig. 3), and it does not emerge from analyses that do not include (direct) information from the SST field (Fig. 5).

We have argued that the pattern of circulation anomalies that follows variations in Gulf Stream extension SSTs is driven by anomalous vertical motion in the region to the northeast of the Gulf Stream extension: for example, positive lower-tropospheric temperature anomalies over the Gulf Stream region are advected northeastward by the climatological flow (Fig. 6) where they are at least partially balanced by anomalous rising motion (Fig. 7). The anomalous rising motion is important, since it suggests heating over the Gulf Stream extension is capable of perturbing the free-tropospheric circulation. It is also robust: a similar pattern of vertical motion anomalies emerges in analyses of the atmospheric response to SST anomalies over the Kuroshio–Oyashio Extension (e.g., Smirnov et al. 2015), and in analyses of the extratropical storm response to SST anomalies in the Gulf Stream region (e.g., Czaja and Blunt 2011; Sheldon and Czaja 2013).

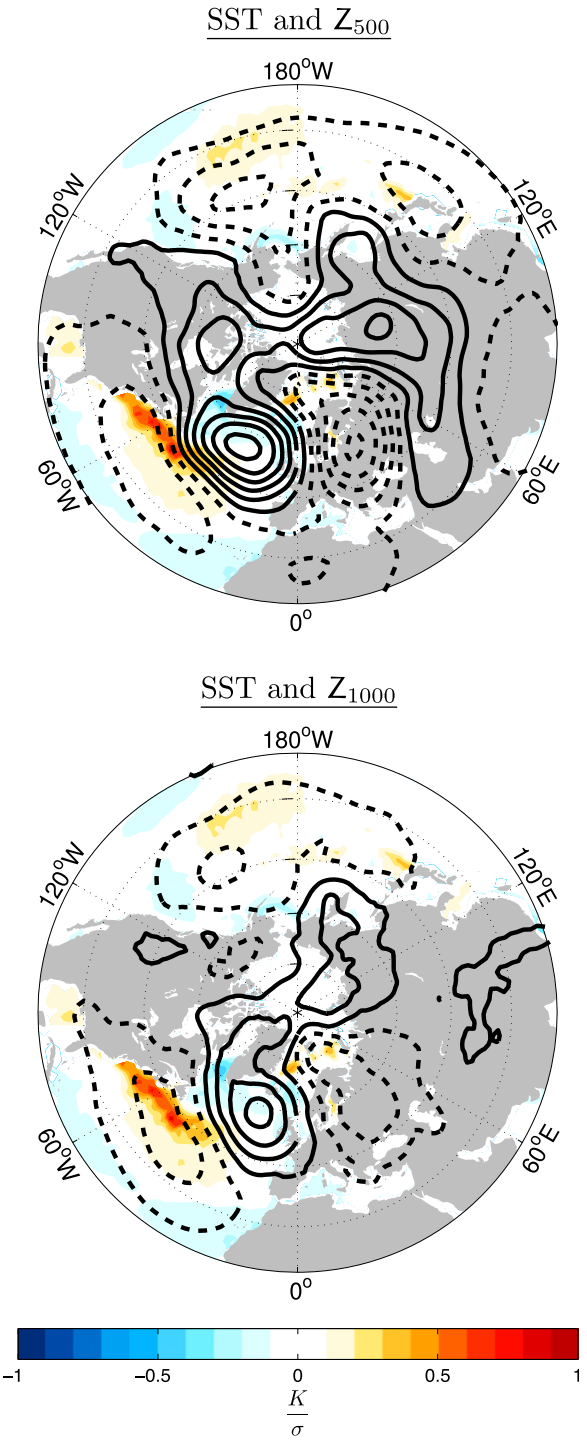

FIG. 8. As in Fig. 2 (bottom left), but for (bottom) SST and Z_{1000} and (top) SST and Z_{500} regressed onto the standardized G_{SST} index over the Northern Hemisphere at a lag of +20 days.

The results shown here are derived from lead–lag analysis of daily mean data. We believe that the use of lag regressions based on daily mean data may provide insight into the nature of extratropical atmosphere–ocean

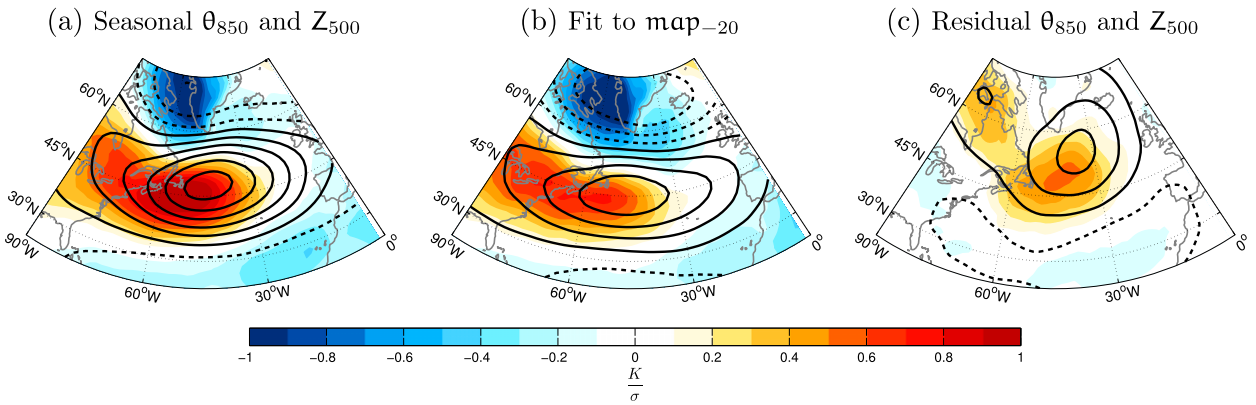

FIG. 9. As in Fig. 4, but for the winter season (NDJFM) monthly mean (a) total regression of θ_{850} (shading) and Z_{500} (contours) onto the standardized monthly mean G_{SST} index. (b),(c) The linear decomposition of the seasonal θ_{850} and Z_{500} anomalies into (b) a linear fit to the −20-day lag pattern (from the daily decomposition in Fig. 4, top left), and (c) a residual. Z_{500} contours are spaced at 6 m (−9, −3, 3, 9, . . . m) where solid (dashed) lines represent positive (negative) values.

coupling in the same way that it has led to new insights into the nature of stratosphere–troposphere coupling (e.g., Baldwin and Dunkerton 2001). The distinction between the patterns of circulation anomalies at negative and positive lags identified here would be much more difficult to extract from regressions based on monthly or seasonal mean data. However, it is interesting to emphasize that both patterns are embedded in such regressions.

For example, the left panel in Fig. 9 shows results derived by regressing winter season [November–March (NDJFM)] monthly mean Z_{500} and θ_{850} anomalies onto standardized, monthly mean values of the G_{SST} index. The middle panel shows the component of the regression map that is linearly congruent with the "atmospheric forcing" pattern, as defined from the lag −20-day regression map shown in Fig. 4. The right panel (the residual of the regression) shows the differences between the left and middle panels. The residual pattern in the right panel bears strong resemblance to the pattern of circulation anomalies that lags variations in G_{SST} on daily time scales. Hence the winter season monthly mean regression map in the left panel reflects the juxtaposition of two distinct patterns of circulation anomalies: the pattern that leads variations in G_{SST} by several weeks, and the pattern that lags variations in G_{SST} by several weeks. We believe the use of daily mean data is key for future analyses of extratropical atmosphere–ocean interaction on subseasonal time scales, and that the results have potential implications for understanding the response of the atmosphere to variations in SSTs on longer time scales.

Acknowledgments. S.M.W. is funded by the NASA Physical Oceanography program under Grant NNX13AQ04G. D.W.J.T. is funded by the NASA Physical Oceanography program and the NSF Climate Dynamics program. L.M.C. is supported by the Centre for Climate Dynamics at the Bjerknes Centre through a grant to the WaCyEx project.

REFERENCES

Baldwin, M. P., and T. J. Dunkerton, 2001: Stratospheric harbingers of anomalous weather regimes. *Science*, **294**, 581–584, doi:10.1126/science.1063315.

Brayshaw, D. J., B. Hoskins, and M. Blackburn, 2008: The storm-track response to idealized SST perturbations in an aquaplanet GCM. *J. Atmos. Sci.*, **65**, 2842–2860, doi:10.1175/2008JAS2657.1.

Bretherton, C. S., M. Widmann, V. P. Dymnikov, J. M. Wallace, and I. Bladé, 1999: The effective number of spatial degrees of freedom of a time-varying field. *J. Climate*, **12**, 1990–2009, doi:10.1175/1520-0442(1999)012<1990:TENOSD>2.0.CO;2.

Chelton, D. B., and S.-P. Xie, 2010: Coupled ocean-atmosphere interaction at oceanic mesoscales. *Oceanography*, **23**, 52–69, doi:10.5670/oceanog.2010.05.

——, M. G. Schlax, M. H. Freilich, and R. F. Milliff, 2004: Satellite measurements reveal persistent small-scale features in ocean winds. *Science*, **303**, 978–983, doi:10.1126/science.1091901.

Ciasto, L. M., and D. W. J. Thompson, 2004: North Atlantic atmosphere–ocean interaction on intraseasonal time scales. *J. Climate*, **17**, 1617–1621, doi:10.1175/1520-0442(2004)017<1617:NAAIOI>2.0.CO;2.

Cui, Y., A. Duan, Y. Liu, and G. Wu, 2015: Interannual variability of the spring atmospheric heat source over the Tibetan Plateau forced by the North Atlantic SSTA. *Climate Dyn.*, **45**, 1617–1634, doi:10.1007/s00382-014-2417-9.

Czaja, A., and C. Frankignoul, 2002: Observed impact of Atlantic SST anomalies on the North Atlantic Oscillation. *J. Climate*, **15**, 606–623, doi:10.1175/1520-0442(2002)015<0606:OIOASA>2.0.CO;2.

——, and N. Blunt, 2011: A new mechanism for ocean-atmosphere coupling in midlatitudes. *Quart. J. Roy. Meteor. Soc.*, **137**, 1095–1101, doi:10.1002/qj.814.

Dee, D. P., and Coauthors, 2011: The ERA-Interim reanalysis: Configuration and performance of the data assimilation system. *Quart. J. Roy. Meteor. Soc.*, **137**, 553–597, doi:10.1002/qj.828.

Deser, C., and M. S. Timlin, 1997: Atmosphere-ocean interaction on weekly timescales in the North Atlantic and Pacific. *J. Climate*, **10**, 393–408, doi:10.1175/1520-0442(1997)010<0393:AOIOWT>2.0.CO;2.

——, M. A. Alexander, S.-P. Xie, and A. S. Phillips, 2010: Sea surface temperature variability: Patterns and mechanisms. *Annu. Rev. Mar. Sci.*, **2**, 115–143, doi:10.1146/annurev-marine-120408-151453.

Frankignoul, C., 1985: Sea surface temperature anomalies, planetary waves, and air–sea feedback in the middle latitudes. *Rev. Geophys.*, **23**, 357–390, doi:10.1029/RG023i004p00357.

——, and R. W. Reynolds, 1983: Testing a dynamical model for mid-latitude sea surface temperature anomalies. *J. Phys. Oceanogr.*, **13**, 1131–1145, doi:10.1175/1520-0485(1983)013<1131:TADMFM>2.0.CO;2.

——, N. Sennechael, Y.-O. Kwon, and M. A. Alexander, 2011: Influence of the meridional shifts of the Kuroshio and the Oyashio Extensions on the atmospheric circulation. *J. Climate*, **24**, 762–777, doi:10.1175/2010JCLI3731.1.

Hand, R., N. Keenlyside, N.-E. Omrani, and M. Latif, 2014: Simulated response to inter-annual SST variations in the Gulf Stream region. *Climate Dyn.*, **42**, 715–731, doi:10.1007/s00382-013-1715-y.

Haney, R. L., 1985: Midlatitude sea surface temperature anomalies: A numerical hindcast. *J. Phys. Oceanogr.*, **15**, 787–799, doi:10.1175/1520-0485(1985)015<0787:MSSTAA>2.0.CO;2.

Horel, J. D., and J. M. Wallace, 1981: Planetary-scale atmospheric phenomena associated with the Southern Oscillation. *Mon. Wea. Rev.*, **109**, 813–829, doi:10.1175/1520-0493(1981)109<0813:PSAPAW>2.0.CO;2.

Hoskins, B. J., and D. J. Karoly, 1981: The steady linear response of a spherical atmosphere to thermal and orographic forcing. *J. Atmos. Sci.*, **38**, 1179–1196, doi:10.1175/1520-0469(1981)038<1179:TSLROA>2.0.CO;2.

Kushnir, Y., W. A. Robinson, I. Blade, N. M. J. Hall, S. Peng, and R. Sutton, 2002: Atmospheric GCM response to extratropical SST anomalies: Synthesis and evaluation. *J. Climate*, **15**, 2233–2256, doi:10.1175/1520-0442(2002)015<2233:AGRTES>2.0.CO;2.

Kwon, Y.-O., and T. M. Joyce, 2013: Northern Hemsiphere winter atmospheric transient eddy heat fluxes and the Gulf Stream and Kuroshio–Oyashio Extension variability. *J. Climate*, **26**, 9839–9859, doi:10.1175/JCLI-D-12-00647.1.

Minobe, S., A. Kuwano-Yoshida, N. Komori, S.-P. Xie, and R. J. Small, 2008: Influence of the Gulf Stream on the troposphere. *Nature*, **452**, 206–210, doi:10.1038/nature06690.

——, M. Miyashita, A. Kuwano-Yoshida, H. Tokinaga, and S.-P. Xie, 2010: Atmospheric response to the Gulf Stream: Seasonal variations. *J. Climate*, **23**, 3699–3719, doi:10.1175/2010JCLI3359.1.

Nakamura, H., G. Lin, and T. Yamagata, 1997: Decadal climate variability in the North Pacific during the recent decades. *Bull. Amer. Meteor. Soc.*, **78**, 2215–2225, doi:10.1175/1520-0477(1997)078<2215:DCVITN>2.0.CO;2.

——, T. Sampe, A. Goto, W. Ohfuchi, and S.-P. Xie, 2008: On the importance of midlatitude oceanic frontal zones for the mean state and dominant variability in the tropospheric circulation. *Geophys. Res. Lett.*, **35**, L15709, doi:10.1029/2008GL034010.

Nakamura, M., and S. Yamane, 2009: Dominant anomaly patterns in the near-surface baroclinicity and accompanying anomalies in the atmosphere and oceans. Part I: North Atlantic basin. *J. Climate*, **22**, 880–904, doi:10.1175/2008JCLI2297.1.

Nonaka, M., and S.-P. Xie, 2003: Covariations of sea surface temperature and wind over the Kuroshio and its extension: Evidence for ocean-to-atmosphere feedback. *J. Climate*, **16**, 1404–1413, doi:10.1175/1520-0442(2003)16<1404:COSSTA>2.0.CO;2.

O'Neill, L. W., D. B. Chelton, and S. K. Esbensen, 2003: Observations of SST-induced perturbations of the wind stress field over the Southern Ocean on seasonal timescales. *J. Climate*, **16**, 2340–2354, doi:10.1175/2780.1.

O'Reilly, C. H., and A. Czaja, 2015: The response of the Pacific storm track and atmospheric circulation to Kuroshio Extension variability. *Quart. J. Roy. Meteor. Soc.*, **141**, 52–66, doi:10.1002/qj.2334.

Piazza, M., L. Terray, J. Boé, E. Maisonnave, and E. Sanchez-Gomez, 2016: Influence of small-scale North Atlantic sea surface temperature patterns on the marine boundary layer and free troposphere: A study using the atmospheric ARPEGE model. *Climate Dyn.*, **46**, 1699–1717, doi:10.1007/s00382-015-2669-z.

Reynolds, R. W., N. A. Rayner, T. M. Smith, D. C. Stokes, and W. Wang, 2002: An improved in situ and satellite SST analysis for climate. *J. Climate*, **15**, 1609–1625, doi:10.1175/1520-0442(2002)015<1609:AIISAS>2.0.CO;2.

Sampe, T., H. Nakamura, A. Goto, and W. Ohfuchi, 2010: Significance of a midlatitude SST frontal zone in the formation of a storm track and an eddy-driven westerly jet. *J. Climate*, **23**, 1793–1814, doi:10.1175/2009JCLI3163.1.

Sheldon, L., and A. Czaja, 2013: Seasonal and interannual variability of an index of deep atmospheric convection over western boundary currents. *Quart. J. Roy. Meteor. Soc.*, **140**, 22–30, doi:10.1002/qj.2103.

Small, R. J., R. A. Tomas, and F. O. Bryan, 2014: Storm track response to ocean fronts in a global high-resolution climate model. *Climate Dyn.*, **43**, 805–828, doi:10.1007/s00382-013-1980-9.

Smirnov, D., M. Newman, and M. A. Alexander, 2014: Investigating the role of ocean–atmosphere coupling in the North Pacific Ocean. *J. Climate*, **27**, 592–606, doi:10.1175/JCLI-D-13-00123.1.

——, ——, ——, Y.-O. Kwon, and C. Frankignoul, 2015: Investigating the local atmospheric response to a realistic shift in the Oyashio sea surface temperature front. *J. Climate*, **28**, 1126–1147, doi:10.1175/JCLI-D-14-00285.1.